Appl. Math. Mech. -Engl. Ed. **31**(5), 593–604 (2010)
DOI 10.1007/s10483-010-0507-9

Applied Mathematics and Mechanics (English Edition)

Mechanics of formation and rupture of human aneurysm*

Jiu-sheng REN (任九生)[1,2], Xue-gang YUAN (袁学刚)[3]

(1. Department of Mechanics, Shanghai University, Shanghai 200444, P. R. China;
2. Shanghai Institute of Applied Mathematics and Mechanics,
Shanghai University, Shanghai 200072, P. R. China;
3. College of Science, Dalian Nationalities University,
Dalian 116600, Liaoning Province, P. R. China)

(Communicated by Xing-ming GUO)

Abstract The mechanical response of the human arterial wall under the combined loading of inflation, axial extension, and torsion is examined within the framework of the large deformation hyper-elastic theory. The probability of the aneurysm formation is explained with the instability theory of structure, and the probability of its rupture is explained with the strength theory of material. Taking account of the residual stress and the smooth muscle activities, a two layer thick-walled circular cylindrical tube model with fiber-reinforced composite-based incompressible anisotropic hyper-elastic materials is employed to model the mechanical behavior of the arterial wall. The deformation curves and the stress distributions of the arterial wall are given under normal and abnormal conditions. The results of the deformation and the structure instability analysis show that the model can describe the uniform inflation deformation of the arterial wall under normal conditions, as well as formation and growth of an aneurysm under abnormal conditions such as the decreased stiffness of the elastic and collagen fibers. From the analysis of the stresses and the material strength, the rupture of an aneurysm may also be described by this model if the wall stress is larger than its strength.

Key words arterial wall with collagen fibers, formation and rupture of aneurysm, residual stress, instability theory of structure, strength theory of material

Chinese Library Classification O343
2000 Mathematics Subject Classification 74B20

1 Introduction

Aneurysms as shown in Fig. 1 have been found in more and more people in the world in recent years[1–5]. Beginning as a small dilatation of the arterial wall, aneurysms can expand to over 10 cm in diameter[2]. Finally, aneurysms may rupture in some cases, occuring at a rate

* Received Jan. 2, 2010 / Revised Apr. 1, 2010
Project supported by the National Natural Science Foundation of China (Nos. 10772104 and 10872045), the Innovation Project of the Shanghai Municipal Education Commission (No. 09YZ12), and the Shanghai Leading Academic Discipline Project (No. S30106)
Corresponding author Jiu-sheng REN, Associate Professor, Ph. D., E-mail: jsren@shu.edu.cn

of 24.9%[2], and this will give rise to terrible consequences at a rate of 90%[3]. The rupture of aneurysms is often followed by the formation of an intraluminal or intramural thrombus[4]. Therefore, some patients die whereas many of the survivors suffer severe functional deficits[4]. At the same time, current aneurysm treatment is expensive and carries considerable morbidity and mortality risks[2–3].

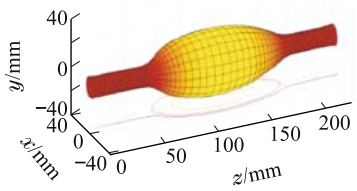

Fig. 1 Schematic representation of an aneurysm[4–5]

There are some theories about the formation or pathogenesis of aneurysms, but little general agreement is obtained[1–3,6–7]. With regard to the rupture of aneurysms, it is widely thought that the rupture occurs when the wall stress of the aneurysm exceeds its strength of the wall following the basic principles of material failure[2–4]. Therefore, it is vital to understand well the mechanism of the aneurysm wall[8–9]. However, the mechanical behaviors of the arterial wall are complex, anisotropic, viscoelastic, and highly nonlinear[1,10–11]. From the histological point of view, the arterial wall is a layered structure composed of three layers: intima, media, and adventitia[12–14]. The contribution of the intima to the mechanical properties of the arterial wall is negligible[14–15]. In the media and adventitia, elastic and collagen fibers are arranged in helically distributed families which induce the anisotropy in the mechanical response of the arterial wall[12,16]. According to Fung[17], most pseudo-elastic constitutive models for the arterial wall are built in the form of exponential and logarithmic strain energy density functions[12,16], while some of the newest constitutive models are built incorporating the histology-derived micro-structure[12,15–16,18–19].

An arterial wall in the load-free configuration is not stress free. If it is cut along a radius, the arterial wall will spring open to form an open sector[17]. That is to say, there are residual stresses and their effect on the stress distribution of the arterial wall should be examined[12,19]. At the same time, when the smooth muscle orientating nearly circumferentially in the media is activated, it will alter circumferential mechanical properties by constricting or dilating[12]. Thus, the active stress due to smooth muscle tone should also be considered[16].

Until recently, biomechanical analysis on the formation, enlargement, and rupture of an aneurysm was scant[8,20] and only a few models had been developed[3,5,21]. Most models are based upon a uniform single-layer circular cylindrical tube and the strain energy function of the material was a simple uniform strain energy function. The growth and the rupture of the aneurysm are studied by most models but the formation of the aneurysm is less mentioned. The purpose of the present paper is to investigate the mechanical response of the arterial wall and try to explain the probability of the formation and rupture of the aneurysm within the framework of the large deformation hyper-elastic theory. The strain energy function used in the paper is for the fiber-reinforced composite-based incompressible anisotropic hyper-elastic material and the smooth muscle activities have been taken into account. Model the arterial wall as a two layer thick-walled circular cylindrical tube and take account of the residual stress. The mechanical response of the arterial wall under the combined loading of inflation, axial extension, and torsion is investigated. The probability of the aneurysm formation is explained with the instability theory of structure, and the probability of its rupture is explained with the strength theory of material. The deformation curves and the stress distributions of the arterial wall are given under normal and abnormal conditions. The results of the deformation and the structure instability analysis show that the model can describe the uniform inflation

deformation of the arterial wall under normal conditions, as well as formation and growth of an aneurysm under abnormal conditions such as the decreased stiffness of the elastic and collagen fibers. From the analysis of the stresses and the material strength, the rupture of the aneurysm may also be described by this model if the wall stress is larger than its strength. The effect of the residual stress, the smooth muscle activity, and the torsion on the mechanical response of the arterial wall and the formation and rupture of an aneurysm are discussed, respectively.

2 Strain energy function

For the typical architecture of the media as shown in Fig. 2, elastic and collagen fibers are arranged in helically distributed families in their orientation. The arterial wall may be modeled

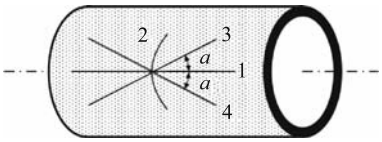

Fig. 2 Schematic representation of the families of elastic and collagen fibers in the media[12]

as an incompressible fiber-reinforced composite material, in which the fibers are viewed as a one-dimensional material, exerting only stress in the fiber direction[12,19],

$$W = W_{\mathrm{M}} + W_{\mathrm{F}} + W_{\mathrm{A}}, \tag{1}$$

where W_{M} is the strain energy of the matrix and is described here by the incompressible Ogden hyper-elastic material[22],

$$W_{\mathrm{M}} = \sum_r \frac{\mu_r}{\alpha_r}\big(\tilde{\lambda}_r^{\alpha_r} + \tilde{\lambda}_\theta^{\alpha_r} + \tilde{\lambda}_z^{\alpha_r} - 3\big), \tag{2}$$

where $\alpha_1 = 1.3, \alpha_2 = 5.0, \alpha_3 = -2.0, \mu_1 = 1.491\mu^{\mathrm{m}}, \mu_2 = 0.003\mu^{\mathrm{m}}$, and $\mu_3 = -0.023\mu^{\mathrm{m}}$; μ^{m} is the shear modulus for the media; $\tilde{\lambda}_r, \tilde{\lambda}_\theta$, and $\tilde{\lambda}_z$ are the principal stretches; and W_{F} is the strain energy of the fibers and is described by the four-fiber family model[12,19],

$$W_{\mathrm{F}} = \sum_{k=1}^{4} \frac{c_{1(k)}}{4c_{2(k)}}\big\{\exp\big[c_{2(k)}(I_{4(k)} - 1)^2\big] - 1\big\}, \tag{3}$$

where material constants $c_{1(k)}$ are the stiffness of the kth family of fibers and $c_{2(k)}$ describe the degree of nonlinearity of the kth family of fibers; $I_{4(k)} = \boldsymbol{M}_{\alpha(k)}\big(\boldsymbol{C}\boldsymbol{M}_{\alpha(k)}\big)$ is the fourth invariant of the right Cauchy-Green deformation tensors, $\boldsymbol{C}$ is the right Cauchy-Green deformation tensor, $\boldsymbol{M}_{\alpha(k)} = [0, \sin\alpha(k), \cos\alpha(k)]$ are the fiber orientations in the reference configuration, and $\alpha(k)$ are the angles between the direction of the kth family of fibers and the axial direction of the arterial wall. For the media shown in Fig. 2, $\alpha(1) = 0^\circ$ for axial fibers, $\alpha(2) = 90^\circ$ for circumferential fibers, $\alpha(3) = \alpha^{\mathrm{m}}$ and $\alpha(4) = -\alpha^{\mathrm{m}}$ for diagonal fibers. W_{A} is the strain energy of the smooth muscles orienting primarily in the circumferential direction[19],

$$W_{\mathrm{A}} = T_{\mathrm{m}}\left[\tilde{\lambda}_\theta + \frac{1}{3}\frac{(\lambda_{\mathrm{m}} - \tilde{\lambda}_\theta)^3}{(\lambda_{\mathrm{m}} - \lambda_{\mathrm{o}})^2}\right], \tag{4}$$

where T_{m} describes the level of activation; λ_{m} is the stretch at which the contraction is a maximum; and λ_{o} is the stretch at which the active force generation ceases.

The strain energy function for the adventitia can be expressed as[12,14]

$$W = W_{\mathrm{M}} + W_{\mathrm{F}}, \tag{5}$$

where W_{M} is the strain energy of the matrix and is also described here by (2) with $\mu_1 = 1.491\mu^{\mathrm{a}}, \mu_2 = 0.003\mu^{\mathrm{a}}, \mu_3 = -0.023\mu^{\mathrm{a}}$; and μ^{a} is the shear modulus for the adventitial. W_{F} is the strain energy of the fibers and is described by the two-fiber family model[12,14]

$$W_{\mathrm{F}} = \sum_{k=1}^{2} \frac{c_{1(k)}}{2c_{2(k)}} \left\{ \exp\left[c_{2(k)} (I_{4(k)} - 1)^2 \right] - 1 \right\}. \tag{6}$$

For the two diagonal fibers of the adventitia, $\alpha(1) = \alpha^{\mathrm{a}}$ and $\alpha(2) = -\alpha^{\mathrm{a}}$.

3 Mathematical formulations

Take account of the residual stress in the arterial wall. The load-free configuration in which the arterial wall is excised from the body and not subjected to any loads is not a stress-free configuration as shown in Fig. 3. Therefore, the open sector is assumed as the undeformed reference configuration[12]. Assume that the stress-free reference configuration, the load-free configuration and the current deformed configuration are described by the cylindrical coordinate systems (R, Θ, Z), (ρ, ϕ, ξ), and (r, θ, z), respectively.

(a) (R, Θ, Z) (b) (ρ, ϕ, ξ) (c) (r, θ, z)

Fig. 3 Kinematics of the arterial wall relative to the stress-free reference configuration (R, Θ, Z), the load-free configuration (ρ, ϕ, ξ), and the current deformed configuration (r, θ, z), respectively[19]

The geometrical region of the stress-free reference configuration is

$$R_{\mathrm{i}} \leqslant R \leqslant R_{\mathrm{o}}, \quad 0 \leqslant \Theta \leqslant 2\Theta_{\mathrm{o}}, \quad 0 \leqslant Z \leqslant L, \tag{7}$$

where $R_{\mathrm{i}}, R_{\mathrm{o}}, \Theta_{\mathrm{o}}$, and L denote the inner and outer radii, the opening angle, and the length of the undeformed tube, respectively. R_{m} denotes the interface between the media and the adventitia. The geometrical region of the current configuration is

$$r_{\mathrm{i}} \leqslant r \leqslant r_{\mathrm{o}}, \quad 0 \leqslant \theta \leqslant 2\pi, \quad 0 \leqslant z \leqslant l, \tag{8}$$

where $r_{\mathrm{i}}, r_{\mathrm{o}}$, and l denote the inner and outer radii and the length of the deformed tube, respectively. The deformation function of the tube subjected to the combined loading of internal inflation, axial extension, and torsion is

$$r = r(R) > 0, \quad \theta = k\Theta + \omega Z, \quad z = \lambda_z Z, \tag{9}$$

where $r(R)$ is a function to be determined, $k = \frac{\pi}{\Theta_{\mathrm{o}}}$ is a measure of the tube opening angle, ω is the torsional angle for unit length, and $\lambda_z = \frac{l}{L}$ is the axial stretch.

Introduce the notations,

$$\lambda_r = \frac{\partial r}{\partial R}, \quad \lambda_\theta = \frac{r}{R}\frac{\partial \theta}{\partial \Theta} = k\frac{r}{R}. \tag{10}$$

Here, $\lambda_r, \lambda_\theta$, and λ_z are the corresponding principal stretches $\tilde{\lambda}_r, \tilde{\lambda}_\theta$, and $\tilde{\lambda}_z$ of the deformation in the radial, circumferential, and axial directions when there is no twist; λ_r is the principal stretch $\tilde{\lambda}_r$ in the radial direction but λ_θ and λ_z are not the principal stretches $\tilde{\lambda}_\theta$ and $\tilde{\lambda}_z$ when there is a twist[12].

The incompressible condition is independent of the twist and requires that

$$\tilde{\lambda}_r\tilde{\lambda}_\theta\tilde{\lambda}_z = \lambda_r\lambda_\theta\lambda_z = 1. \tag{11}$$

Then, the corresponding deformation-gradient tensor $\boldsymbol{F}$ is

$$\boldsymbol{F} = \begin{pmatrix} (\lambda_\theta\lambda_z)^{-1} & 0 & 0 \\ 0 & \lambda_\theta & r\omega \\ 0 & 0 & \lambda_z \end{pmatrix}. \tag{12}$$

The corresponding right and left Cauchy-Green deformation tensors are

$$\boldsymbol{C} = \begin{pmatrix} (\lambda_\theta\lambda_z)^{-2} & 0 & 0 \\ 0 & \lambda_\theta^2 & r\omega\lambda_\theta \\ 0 & r\omega\lambda_\theta & \lambda_z^2 + (r\omega)^2 \end{pmatrix}, \tag{13}$$

$$\boldsymbol{B} = \begin{pmatrix} (\lambda_\theta\lambda_z)^{-2} & 0 & 0 \\ 0 & \lambda_\theta^2 + (r\omega)^2 & r\omega\lambda_z \\ 0 & r\omega\lambda_z & \lambda_z^2 \end{pmatrix}. \tag{14}$$

The equilibrium equations for the tube in the absence of body forces are

$$\frac{d\sigma_{rr}^{\mathrm{m}}}{dR} + \frac{\dot{r}(R)}{r(R)}\left(\sigma_{rr}^{\mathrm{m}} - \sigma_{\theta\theta}^{\mathrm{m}}\right) = 0, \quad R_{\mathrm{i}} \leqslant R \leqslant R_{\mathrm{m}}, \tag{15a}$$

$$\frac{d\sigma_{rr}^{\mathrm{a}}}{dR} + \frac{\dot{r}(R)}{r(R)}\left(\sigma_{rr}^{\mathrm{a}} - \sigma_{\theta\theta}^{\mathrm{a}}\right) = 0, \quad R_{\mathrm{m}} \leqslant R \leqslant R_{\mathrm{o}}, \tag{15b}$$

where $\dot{r}(R) = \frac{dr}{dR}$, σ_{rr}^{m}, $\sigma_{\theta\theta}^{\mathrm{m}}$, and σ_{zz}^{m} represent the Cauchy stress components of the media, and $\sigma_{rr}^{\mathrm{a}}, \sigma_{\theta\theta}^{\mathrm{a}}$, and σ_{zz}^{a} represent the Cauchy stress components of the adventitia, respectively. Without special announcing in this paper, the superscript m denotes the media part and the superscript a denotes the a dventitia part. The boundary conditions are

$$\sigma_{rr}^{\mathrm{m}} = -q, \quad R = R_{\mathrm{i}}, \quad \sigma_{rr}^{\mathrm{a}} = 0, \quad R = R_{\mathrm{o}}, \tag{16}$$

where q is the internal inflation pressure.

From the continuity of σ_{rr} at the interface of the media and the adventitia,

$$\sigma_{rr}^{\mathrm{m}} = \sigma_{rr}^{\mathrm{a}}, \quad R = R_{\mathrm{m}}. \tag{17}$$

4 Solutions

The incompressible condition of the material (11) can be expressed as

$$r(R) = \left[\frac{1}{k\lambda_z}\left(R^2 - R_{\mathrm{i}}^2\right) + r_{\mathrm{i}}^2\right]^{\frac{1}{2}}. \tag{18}$$

Then

$$\lambda_\theta = k\left[\frac{1}{k\lambda_z}\left(1 - \frac{R_{\mathrm{i}}^2}{R^2}\right) + \frac{r_{\mathrm{i}}^2}{R^2}\right]^{\frac{1}{2}}, \tag{19}$$

$$I_4(k) = \sin^2\alpha(k)\lambda_\theta^2 + 2\sin\alpha(k)\cos\alpha(k)r\omega\lambda_\theta + \cos^2\alpha(k)[\lambda_z^2 + (r\omega)^2]. \tag{20}$$

The non-zero Cauchy stresses for the media are

$$\sigma_{rr}^{\mathrm{m}}(R) = -p^{\mathrm{m}}(R) + \sum_r \mu_{\alpha_r}{}^{\mathrm{m}}\lambda_z^{-\alpha_r}\lambda_\theta^{-\alpha_r}, \tag{21a}$$

$$\sigma_{\theta\theta}^{\mathrm{m}}(R) = -p^{\mathrm{m}}(R) + \sum_r \mu_{\alpha_r}^{\mathrm{m}}[\lambda_\theta^2 + (r\omega)^2]^{\frac{\alpha_r}{2}} + \sum_{k=1}^{4} c_{1(k)}^{\mathrm{m}}(I_{4(k)} - 1)\exp[c_{2(k)}^{\mathrm{m}}(I_{4(k)} - 1)^2](\sin\alpha(k)\lambda_\theta$$
$$+ \cos\alpha(k)r\omega)^2 + T_{\mathrm{m}}[\lambda_\theta^2 + (r\omega)^2]^{\frac{1}{2}}\left[1 - \left(\frac{\lambda_{\mathrm{m}} - (\lambda_\theta^2 + (r\omega)^2)^{\frac{1}{2}}}{\lambda_{\mathrm{m}} - \lambda_{\mathrm{o}}}\right)^2\right], \tag{21b}$$

$$\sigma_{zz}^{\mathrm{m}}(R)=-p^{\mathrm{m}}(R)+\sum_r \mu_{\alpha_r}^{\mathrm{m}}\lambda_z^{\alpha_r}+\sum_{k=1}^{4} c_{1(k)}^{\mathrm{m}}(I_{4(k)}-1)\exp[c_{2(k)}^{\mathrm{m}}(I_{4(k)}-1)^2]\cos^2\alpha(k)\lambda_z^2, \quad (21c)$$

$$\frac{1}{r}\sigma_{\theta z}^{\mathrm{m}}(R)=\sum_r \mu_{\alpha_r}^{\mathrm{m}}(r\omega\lambda_z)^{\frac{\alpha_r}{2}}+\sum_{k=1}^{4} c_{1(k)}^{\mathrm{m}}(I_{4(k)}-1)\exp[c_{2(k)}^{\mathrm{m}}(I_{4(k)}-1)^2]$$
$$\cdot(\sin\alpha(k)\lambda_\theta+\cos\alpha(k)r\omega)\cos\alpha(k)\lambda_z. \quad (21d)$$

The non-zero Cauchy stresses for the adventitia are

$$\sigma_{rr}^{\mathrm{a}}(R)=-p^{\mathrm{a}}(R)+\sum_r \mu_{\alpha_r}^{\mathrm{a}}\lambda_z^{-\alpha_r}\lambda_\theta^{-\alpha_r}, \quad (22a)$$

$$\sigma_{\theta\theta}^{\mathrm{a}}(R)=-p^{\mathrm{a}}(R)+\sum_r \mu_{\alpha_r}^{\mathrm{a}}[\lambda_\theta^2+(r\omega)^2]^{\frac{\alpha_r}{2}}+2\sum_{k=1}^{2} c_{1(k)}^{\mathrm{a}}(I_{4(k)}-1)\exp[c_{2(k)}^{\mathrm{a}}(I_{4(k)}-1)^2]$$
$$\cdot(\sin\alpha(k)\lambda_\theta+\cos\alpha(k)r\omega)^2, \quad (22b)$$

$$\sigma_{zz}^{\mathrm{a}}(R)=-p^{\mathrm{a}}(R)+\sum_r \mu_{\alpha_r}^{\mathrm{a}}\lambda_z^{\alpha_r}+2\sum_{k=1}^{2} c_{1(k)}^{\mathrm{a}}(I_{4(k)}-1)\exp[c_{2(k)}^{\mathrm{a}}(I_{4(k)}-1)^2]\cos^2\alpha(k)\lambda_z^2, \quad (22c)$$

$$\frac{1}{r}\sigma_{\theta z}^{\mathrm{a}}(R)=\sum_r \mu_{\alpha_r}^{\mathrm{a}}(r\omega\lambda_z)^{\frac{\alpha_r}{2}}+2\sum_{k=1}^{2} c_{1(k)}^{\mathrm{a}}(I_{4(k)}-1)\exp[c_{2(k)}^{\mathrm{a}}(I_{4(k)}-1)^2]$$
$$\cdot(\sin\alpha(k)\lambda_\theta+\cos\alpha(k)r\omega)\cos\alpha(k)\lambda_z, \quad (22d)$$

where $p^{\mathrm{m}}(R)$ and $p^{\mathrm{a}}(R)$ are the hydrostatic pressures. Substituting stresses (21) and (22) into equations (15a), (15b) and integrating them over radius R from the inner wall R_{i} with the conditions (16) and (17), we have $p^{\mathrm{m}}(R_{\mathrm{i}})=p^{\mathrm{a}}(R_{\mathrm{i}})=p(R_{\mathrm{i}})=q$ and

$$\begin{aligned} q=&-\int_{R_{\mathrm{i}}}^{R_{\mathrm{m}}}\frac{R}{k\lambda_z r^2\omega^2}\Big\{\sum_r \mu_{\alpha_r}^{\mathrm{m}}\big[\lambda_z^{-\alpha_r}\lambda_\theta^{-\alpha_r}-(\lambda_\theta^2+r^2\omega^2)^{\frac{\alpha_r}{2}}\big]\\ &-\sum_{k=1}^{4} c_{1(k)}^{\mathrm{m}}(I_{4(k)}-1)\exp[c_{2(k)}^{\mathrm{m}}(I_{4(k)}-1)^2](\sin\alpha(k)\lambda_\theta+\cos\alpha(k)r\omega)^2\\ &-T_{\mathrm{m}}(\lambda_\theta^2+(r\omega)^2)^{\frac{1}{2}}\Big[1-\Big(\frac{\lambda_{\mathrm{m}}-(\lambda_\theta^2+(r\omega)^2)^{\frac{1}{2}}}{\lambda_{\mathrm{m}}-\lambda_{\mathrm{o}}}\Big)^2\Big]\Big\}dR\\ &-\int_{R_{\mathrm{m}}}^{R_{\mathrm{o}}}\frac{R}{k\lambda_z r^2\omega^2}\Big\{\sum_r \mu_{\alpha_r}^{\mathrm{a}}\big[\lambda_z^{-\alpha_r}\lambda_\theta^{-\alpha_r}-(\lambda_\theta^2+r^2\omega^2)^{\frac{\alpha_r}{2}}\big]\\ &-\sum_{k=1}^{2} c_{1(k)}^{\mathrm{a}}(I_{4(k)}-1)\exp\big[c_{2(k)}^{\mathrm{a}}(I_{4(k)}-1)^2\big](\sin\alpha(k)\lambda_\theta+\cos\alpha(k)r\omega)^2\Big\}dR. \end{aligned} \quad (23)$$

For a given value of the inflation pressure, an exact value for the deformed internal radius will be determined from (23) and the deformation of the tube will be described.

The corresponding non-zero stresses for the media are

$$\begin{aligned} \sigma_{rr}^{\mathrm{m}}=&-q-\int_{R_{\mathrm{i}}}^{R}\frac{R}{k\lambda_z r^2\omega^2}\Big\{\sum_r \mu_{\alpha_r}^{\mathrm{m}}[\lambda_z^{-\alpha_r}\lambda_\theta^{-\alpha_r}-(\lambda_\theta^2+r^2\omega^2)^{\frac{\alpha_r}{2}}]\\ &-\sum_{k=1}^{4} c_{1(k)}^{\mathrm{m}}(I_{4(k)}-1)\exp[c_{2(k)}^{\mathrm{m}}(I_{4(k)}-1)^2](\sin\alpha(k)\lambda_\theta+\cos\alpha(k)r\omega)^2\\ &-T_{\mathrm{m}}(\lambda_\theta^2+(r\omega)^2)^{\frac{1}{2}}\Big[1-\Big(\frac{\lambda_{\mathrm{m}}-(\lambda_\theta^2+(r\omega)^2)^{\frac{1}{2}}}{\lambda_{\mathrm{m}}-\lambda_{\mathrm{o}}}\Big)^2\Big]\Big\}dR, \end{aligned} \quad (24a)$$

$$\begin{aligned} \sigma_{\theta\theta}^{\mathrm{m}}=&-\sum_r \mu_{\alpha_r}^{\mathrm{m}}\Big[\lambda_z^{-\alpha_r}\lambda_\theta^{-\alpha_r}-(\lambda_\theta^2+r^2\omega^2)^{\frac{\alpha_r}{2}}\Big]+\sum_{k=1}^{4} c_{1(k)}^{\mathrm{m}}(I_{4(k)}-1)\exp[c_{2(k)}^{\mathrm{m}}(I_{4(k)}-1)^2]\\ &\cdot(\sin\alpha(k)\lambda_\theta+\cos\alpha(k)r\omega)^2+T_{\mathrm{m}}[\lambda_\theta^2+(r\omega)^2]^{\frac{1}{2}}\Big\{1-\Big[\frac{\lambda_{\mathrm{m}}-(\lambda_\theta^2+(r\omega)^2)^{\frac{1}{2}}}{\lambda_{\mathrm{m}}-\lambda_{\mathrm{o}}}\Big]^2\Big\}+\sigma_{rr}^{\mathrm{m}}, \end{aligned} \quad (24b)$$

$$\sigma_{zz}^{\mathrm{m}}=\sum_r \mu_{\alpha_r}^{\mathrm{m}}(\lambda_z^{\alpha_r}-\lambda_z^{-\alpha_r}\lambda_\theta^{-\alpha_r})+\sum_{k=1}^{4} c_{1(k)}^{\mathrm{m}}(I_{4(k)}-1)\exp[c_{2(k)}^{\mathrm{m}}(I_{4(k)}-1)^2]\cos^2\alpha(k)\lambda_z^2+\sigma_{rr}^{\mathrm{m}}, \quad (24c)$$

$$\frac{1}{r}\sigma_{\theta z}^{\mathrm{m}} = \sum_r \mu_{\alpha_r}^{\mathrm{m}}\left[(r\lambda_z)^{\frac{\alpha_r}{2}}-\lambda_z^{-\alpha_r}\lambda_\theta^{-\alpha_r}\right]+\sum_{k=1}^{4} c_{1(k)}^{\mathrm{m}}(I_{4(k)}-1)\exp[c_{2(k)}^{\mathrm{m}}(I_{4(k)}-1)^2]$$
$$\cdot(\sin\alpha(k)\lambda_\theta+\cos\alpha(k)r\omega)\cos\alpha(k)\lambda_z+\sigma_{rr}^{\mathrm{m}}+q. \quad (24d)$$

The corresponding non-zero stresses for the adventitia are

$$\sigma_{rr}^{\mathrm{a}} = -q-\int_{R_{\mathrm{i}}}^{R_{\mathrm{m}}}\frac{R}{k\lambda_z r^2\omega^2}\Big\{\sum_r \mu_{\alpha_r}^{\mathrm{m}}[\lambda_z^{-\alpha_r}\lambda_\theta^{-\alpha_r}-(\lambda_\theta^2+r^2\omega^2)^{\frac{\alpha_r}{2}}]$$
$$-\sum_{k=1}^{4} c_{1(k)}^{\mathrm{m}}(I_{4(k)}-1)\exp[c_{2(k)}^{\mathrm{m}}(I_{4(k)}-1)^2](\sin\alpha(k)\lambda_\theta+\cos\alpha(k)r\omega)^2$$
$$-T_{\mathrm{m}}(\lambda_\theta^2+(r\omega)^2)^{\frac{1}{2}}\left[1-\left(\frac{\lambda_{\mathrm{m}}-(\lambda_\theta^2+(r\omega)^2)^{\frac{1}{2}}}{\lambda_{\mathrm{m}}-\lambda_{\mathrm{o}}}\right)^2\right]\Big\}dR$$
$$-\int_{R_{\mathrm{m}}}^{R}\frac{R}{k\lambda_z r^2\omega^2}\Big\{\sum_r \mu_{\alpha_r}^{\mathrm{a}}\left[\lambda_z^{-\alpha_r}\lambda_\theta^{-\alpha_r}-(\lambda_\theta^2+r^2\omega^2)^{\frac{\alpha_r}{2}}\right]$$
$$-2\sum_{k=1}^{2} c_{1(k)}^{\mathrm{a}}(I_{4(k)}-1)\exp[c_{2(k)}^{\mathrm{a}}(I_{4(k)}-1)^2](\sin\alpha(k)\lambda_\theta+\cos\alpha(k)r\omega)^2\Big\}dR, \quad (25a)$$

$$\sigma_{\theta\theta}^{\mathrm{a}} = -\sum_r \mu_{\alpha_r}^{\mathrm{a}}\left[\lambda_z^{-\alpha_r}\lambda_\theta^{-\alpha_r}-(\lambda_\theta^2+r^2\omega^2)^{\frac{\alpha_r}{2}}\right]+2\sum_{k=1}^{2} c_{1(k)}^{\mathrm{a}}(I_{4(k)}-1)\exp[c_{2(k)}^{\mathrm{a}}(I_{4(k)}-1)^2]$$
$$\cdot(\sin\alpha(k)\lambda_\theta+\cos\alpha(k)r\omega)^2+\sigma_{rr}^{\mathrm{a}}, \quad (25b)$$

$$\sigma_{zz}^{\mathrm{a}} = \sum_r \mu_{\alpha_r}^{\mathrm{a}}\left(\lambda_z^{\alpha_r}-\lambda_z^{-\alpha_r}\lambda_\theta^{-\alpha_r}\right)+2\sum_{k=1}^{2} c_{1(k)}^{\mathrm{a}}(I_{4(k)}-1)\exp[c_{2(k)}^{\mathrm{a}}(I_{4(k)}-1)^2]$$
$$\cdot\cos^2\alpha(k)\lambda_z^2+\sigma_{rr}^{\mathrm{a}}, \quad (25c)$$

$$\frac{1}{r}\sigma_{\theta z}^{\mathrm{a}} = \sum_r \mu_{\alpha_r}^{\mathrm{a}}\left[(r\lambda_z)^{\frac{\alpha_r}{2}}-\lambda_z^{-\alpha_r}\lambda_\theta^{-\alpha_r}\right]+2\sum_{k=1}^{2} c_{1(k)}^{\mathrm{a}}(I_{4(k)}-1)\exp[c_{2(k)}^{\mathrm{a}}(I_{4(k)}-1)^2]$$
$$\cdot(\sin\alpha(k)\lambda_\theta+\cos\alpha(k)r\omega)\cos\alpha(k)\lambda_z+\sigma_{rr}^{\mathrm{a}}+q. \quad (25d)$$

5 Results and analysis

The reference values for the geometrical and material parameters as well as the loading conditions used in calculations are summarized in Table 1[23–24].

5.1 Deformation and stresses under normal conditions

Expression (23) gives the stretch-inflation pressure curves for the arterial wall under normal conditions that are shown in Fig. 4. Expressions (24) and (25) yield the values of stresses for the arterial wall. Distribution of stresses for the arterial wall under a certain normal condition ($\lambda_z = 1.09,\ q = 13.67$ kPa) is shown in Fig. 5 and varieties of stresses with internal pressure (probability for the fluctuation of the blood pressure) for the internal wall are shown in Fig. 6. In the following figures, x is defined as $x = \frac{r_{\mathrm{i}}}{R_{\mathrm{i}}}$, which describes the deformation of the inner radius.

As shown in Fig. 4, under normal conditions, deformation curves are monotone. That is to say, the arterial wall takes up a uniform inflation and there are no aneurysms under normal conditions. The effects of residual stress and the smooth muscle activity are evident, and the arterial wall will have a larger inflation if their effects are neglected. In addition, the effect of

Table 1 Reference values of the parameters used in the model

Parameter	Description	Value
R_{i}	Inner radius (stress-free configuration)	3.302/mm
R_{m}	Interface for the media and adventitia	3.795/mm
R_{o}	Outer radius	4.042/mm
μ_{m}	Shear modulus for the media	43.48/kPa
μ_{a}	Shear modulus for the adventitia	2.7/kPa
$c^{\mathrm{m}}_{1(1,3,4)}$	Stiffness parameter for the 1^{st}, 3^{rd}, 4^{th} fiber families of the media	22.84/kPa
$c^{\mathrm{m}}_{2(1,3,4)}$	Nonlinearity parameter for the 1^{st}, 3^{rd}, 4^{th} fiber families of the media	13.20
$c^{\mathrm{m}}_{1(2)}$	Stiffness parameter for the 2^{nd} fiber families of the media	11.76/kPa
$c^{\mathrm{m}}_{2(2)}$	Nonlinearity parameter for the 2^{nd} fiber families of the media	12.99
$c^{\mathrm{a}}_{1(1,2)}$	Stiffness parameter for the 1^{st}, 2^{nd} fiber families of the adventitia	5.1/kPa
$c^{\mathrm{a}}_{2(1,2)}$	Nonlinearity parameter for the 1^{st}, 2^{nd} fiber families of the adventitia	15.4
Θ_{o}	Opening angle	130.9/(°)
λ_z	Axial stretch	1.6–1.0
α^{m}	Initial direction for the diagonal fibers of the media	51.2/(°)
α^{a}	Initial direction for the diagonal fibers of the adventitia	40/(°)
T_{m}	Activation level of the smooth muscle of the media	49.89/kPa
λ_{o}	Minimum stretch possible	0.89
λ_{m}	Maximum contraction stretch	1.62

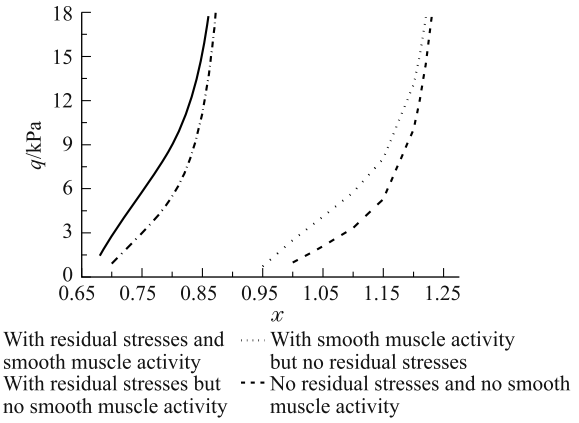

Fig. 4 Deformation of the internal arterial wall vs. internal pressure

residual stress is more severe than that of the smooth muscle activity. As for the torsion, differences between different results are so small that its effect can be ignored.

Figures 5 and 6 show that the circumferential stress and the axial stress increase with the increasing of radius. They are discontinuous with a catastrophic jumping at the interface of the media and the adventitia, and they are much larger in the media than in the adventitia. This phenomenon of the discontinuity of the circumferential stress and the axial stress is caused by the two layer model[13,24]. The absolute value for the radial stress decreases with the increase of the radius. It is continuous and zero at the outer surface. In addition, all the stress components increase with the increase of the pressure.

5.2 Formation and rupture of aneurysm under abnormal conditions

Abnormal conditions such as the decrease of the stiffness of the collagen fibers and the decrease of the matrix modulus properly related to age or vascular disease are considered here[6]. Deformation curves for the arterial wall under three abnormal conditions are shown in Fig. 7 and the varieties of stresses for the internal wall under abnormal condition 3 are shown in

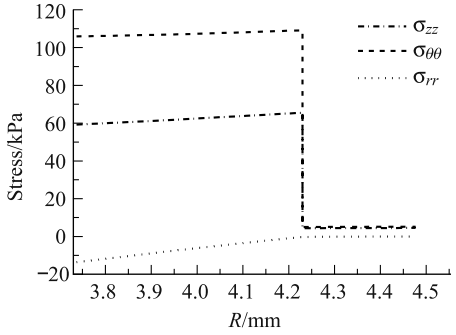

Fig. 5 Stress distribution for the arterial wall ($\lambda_z = 1.09$ and $q = 13.67$ kPa)

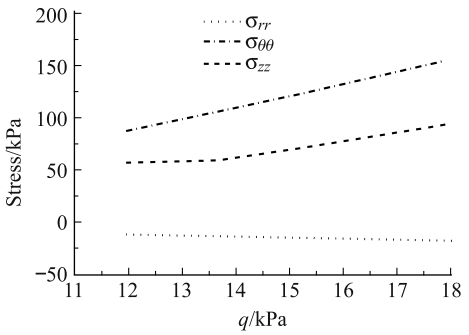

Fig. 6 Stresses of the internal wall vs. internal pressure ($\lambda_z = 1.09$)

Fig. 8, respectively. For the abnormal condition 1, $c^{\mathrm{m}}_{1(k)} = 0$, $c^{\mathrm{a}}_{1(k)} = 0$. For abnormal condition 2, $c^{\mathrm{m}}_{1(1,3,4)} = \frac{22.84}{300}$ kPa, $c^{\mathrm{m}}_{1(2)} = \frac{11.76}{300}$ kPa, $c^{\mathrm{a}}_{1(k)} = \frac{5.4}{300}$ kPa. For abnormal condition 3, $c^{\mathrm{m}}_{1(1,3,4)} = \frac{22.84}{200}$ kPa, $c^{\mathrm{m}}_{1(2)} = \frac{11.76}{200}$ kPa, $c^{\mathrm{a}}_{1(k)} = \frac{5.4}{200}$ kPa.

The decrease of the shear modulus of the matrix does not give rise to much change of the deformation curves and its main difference with respect to the normal condition on the curves is at the small strain deformation stage.

The deformation curve changes with the change of the stiffness of the collagen fibers as shown in Fig. 7. It is shown that there exists a maximum pressure $q_{1\mathrm{cr}}\,(x = x_1)$ on the deformation curves. When the pressure is less than the maximum pressure, the circumferential stretch of the arterial wall increases gradually with the increase of the pressure and the deformation matches along with the internal pressure one by one. However, when the pressure is larger than this maximum pressure, the stretch can increase rapidly even if the pressure is unchanged or decreases and the deformation does not match along with the internal pressure one by one.

As shown in Fig. 8, the circumferential stress, the axial stress, and the radial stress all increase with the increase of the pressure. The circumferential stress increases much quickly in the high deformation stage. Under the same inflation pressure, there will be a larger inflation and a much larger circumferential stress for the abnormal conditions than that for the normal conditions.

As shown in the deformation curves of the arterial wall in Fig. 7, there are more than one solutions corresponding to different inflations for a certain pressure, so that the instability is encountered, and it is necessary to compare the total potential energy for the arterial wall. The total potential energy of the inflated tube with internal inflation pressure from the initial stress-free state is

$$\begin{aligned} E &= \int_V W dV - \int_A q(r(R_{\mathrm{o}}) - R_{\mathrm{o}}) dA = 2\pi L \int_{R_{\mathrm{i}}}^{R_{\mathrm{o}}} RW dR - \pi L q(r^2(R_{\mathrm{o}}) - R_{\mathrm{o}}^2) \\ &= 2\pi L \int_{R_{\mathrm{i}}}^{R_{\mathrm{m}}} R\left[\sum_r^3 \frac{\mu_r^{\mathrm{m}}}{\alpha_r}(\lambda_\theta^{-\alpha_r}\lambda_z^{-\alpha_r} + \lambda_\theta^{\alpha_r} + \lambda_z^{\alpha_r} - 3)\right] dR \\ &\quad + 2\pi L \int_{R_{\mathrm{m}}}^{R_{\mathrm{o}}} R\left[\sum_r^3 \frac{\mu_r^{\mathrm{a}}}{\alpha_r}(\lambda_\theta^{-\alpha_r}\lambda_z^{-\alpha_r} + \lambda_\theta^{\alpha_r} + \lambda_z^{\alpha_r} - 3)\right] dR - \pi L q(r^2(R_{\mathrm{o}}) - R_{\mathrm{o}}^2). \end{aligned} \tag{26}$$

The numerical results of (26) for the inflated arterial wall under abnormal condition 4 of $T_{\mathrm{m}} = 0, c^{\mathrm{m}}_{1(k)} = 0$, and $c^{\mathrm{a}}_{1(k)} = 0$ with no residual stress and the corresponding deformation curve are shown in Figs. 9 and 10, respectively. It is shown that the total potential energy of the inflated arterial wall decreases with the increase of the stretch when $x \leqslant x_1$ or $x_2 \leqslant x$. However, it increases with the increase of stretch when $x_1 \leqslant x \leqslant x_2$. The total potential energy

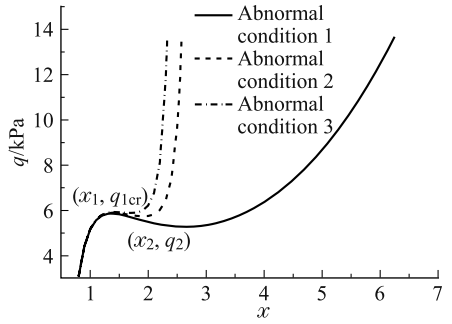

Fig. 7 Deformation of the internal arterial wall vs. internal pressure under abnormal conditions

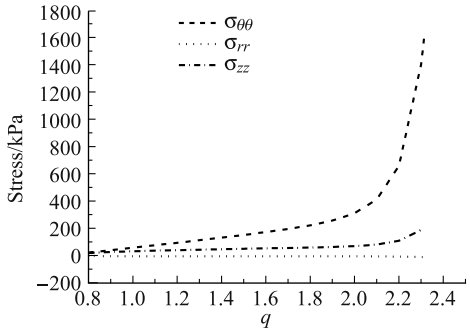

Fig. 8 Stresses of the internal wall vs. internal pressure under abnormal condition 3

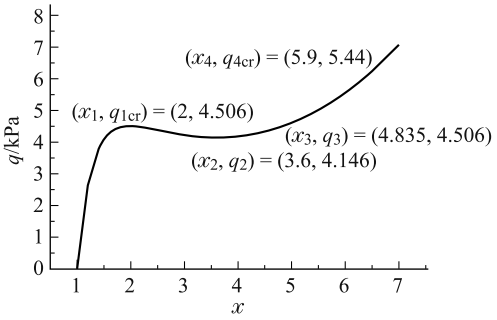

Fig. 9 Deformation of the internal arterial wall vs. internal pressure under abnormal condition 4

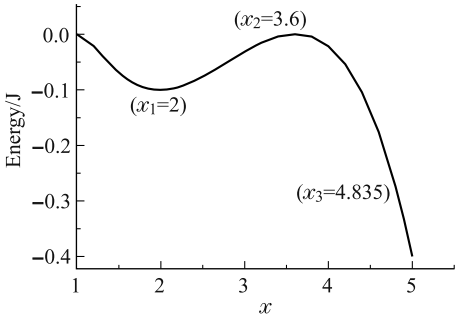

Fig. 10 Energy curve under abnormal condition 4

at stretch $x_3 = 4.835$ is less than that at stretch $x_1 = 2.0$ under the same inflation pressure $q = 4.506$ kPa. That is to say, the arterial wall attains a stable deformation state when the pressure is less than the maximum pressure and takes up a uniform deformation. However, when the pressure is larger than the maximum pressure, the deformation state is unstable. The arterial wall is subject to a complex deformation. One part of the arterial wall becomes highly distended like a bubble[4–5]. This means that an aneurysm is formed in the arterial wall. When the stretch reaches the value of $x_3 = 4.835$, the arterial wall will attain a second stable deformation. The stretch will increase with the increase pressure again. The aneurysm will expand after its formation, then it will expand to a certain extent until the final rupture[4].

It is widely thought that the rupture criterion should be based on the local multi-axial states of stress[6]. If the stress induced by pressure is less than the strength of the arterial wall, the aneurysm will keep its inflation state. However, if this stress is larger than the strength of the arterial wall, the rupture will occur. Based on the observation of Humphrey[4], two human secular aneurysms rupture if the critical stress σ_c ranging from 1 MPa to 2 MPa, and here $\sigma_c = 1.6$ MPa is introduced to model the rupture of the aneurysm.

For all the discussed cases with the probability for the formation of an aneurysm, the critical pressure q_{1cr} corresponding to the formation of an aneurysm, and the critical breaking pressure q_{4cr} along with the corresponding inflation deformations are shown in Table 2.

It is shown that the critical pressures q_{1cr} corresponding to the formation of an aneurysm are different under different abnormal conditions but they are all less than the normal blood pressure $q = 13.67$ kPa. The formation of an aneurysm is possible under certain abnormal

Table 2 Critical pressures and the corresponding inflation deformations

	Condition 1	Condition 2	Condition 3	Condition 4
$q_{1\mathrm{cr}}$/kPa	5.862	5.909	5.933	4.506
x_1	1.350	1.400	1.400	2.000
$q_{4\mathrm{cr}}$/kPa, $\sigma_{\mathrm{c}} = 1.6$ MPa	6.958	11.150	12.850	5.440
x_4	4.300	2.535	2.316	5.900
$q_{4\mathrm{cr}}$/kPa, $\sigma_{\mathrm{c}} = 2.0$ MPa	7.590	12.610	14.530	5.950

conditions. At the same time, the radius of the aneurysm when it is formed under different abnormal conditions is different.

It is also shown that the critical breaking pressure $q_{4\mathrm{cr}}$ corresponding to the rupture of aneurysms is different under different abnormal conditions. If $\sigma_{\mathrm{c}} = 1.6$ MPa is taken out to model the rupture of the aneurysm, the normal blood pressure $q = 13.67$ kPa is large enough for the rupture of the aneurysms. However, if $\sigma_{\mathrm{c}} = 2.0$ MPa is taken out, the normal blood pressure $q = 13.67$ kPa is not large enough for the rupture of the aneurysm under abnormal condition 3. Thus, the aneurysm will keep its inflation state without the risk of rupture. The radius of the aneurysm when it is ruptured under different abnormal conditions is also different.

Therefore, aneurysms may be formed in arteries under some conditions if the stiffness of the collagen fibers decreases to a certain degree properly due to age or vascular disease. The aneurysms may expand to a much large extent and some may catastrophically rupture if the stress is larger than the strength of the arterial wall. However, others may keep their inflation states and they may have different radii.

6 Conclusions

The formation, enlargement, and rupture of an aneurysm in the arterial wall can be described by the model presented in this paper and the effect of other factor is discussed. Aneurysms can be formed in the arterial wall under some abnormal conditions if the stiffness of the collagen fibers decreases to a certain degree. Aneurysms may undergo instable and stable expand deformations and it can expand to a much large extent. Finally, some aneurysms may catastrophically rupture if the stress induced by the pressure is larger than the strength of the arterial wall. However, some aneurysms may keep their inflation states and they may have different radii. The effect of collagen fibers distributed in the arterial wall is remarkable. It affects the formation, enlargement, and rupture of the aneurysm. The effect of residual stress and the smooth muscle activity is evident, and the arterial wall will have a larger inflation if this effect is neglected. The effect of the torsion on the inflation of the arterial wall can be ignored.

However, the arterial wall has been modeled as a perfectly straight cylindrical tube. Hence, it cannot describe curved arteries. The circumferential stress and the axial stress obtained from this two layer model are discontinuous at the interface of the media and the adventitia, and the three dimensional residue stresses should be considered into the model. The formation of an aneurysm can be described but where aneurysms are most likely to occur and the shape of aneurysms cannot be explained. Otherwise, there is less combination with pathology and physiology. To understand well the formation and rupture of aneurysms, it is necessary to combine mechanical and histological methods with clinical diagnosis and treatment, and it is our next effort.

References

[1] Humphrey, J. D. *Cardiovascular Solid Mechanics, Cells, Tissues and Organs*, Springer-Verlag, New York (2002)

[2] Vorp, D. A. Biomechanics of abdominal aortic aneurysm. *Journal of Biomechanics* **40**(9), 1887–1902 (2007)

[3] Volokh, K. Y. and Vorp, D. A. A model of growth and rupture of abdominal aortic aneurysm. *Journal of Biomechanics* **41**(5), 1015–1021 (2008)

[4] Humphrey, J. D. Continuum biomechanics of soft biological tissues. *Proceedings of the Royal Society A*: *Mathematical*, *Physical and Engineering Sciences* **459**(1), 3–46 (2003)

[5] Watton, P. N., Hill, N. A., and Heil, M. A mathematical model for the growth of abdominal aortic aneurysm. *Biomechanics and Modeling in Mechanobiology* **3**(2), 98–113 (2004)

[6] Humphrey, J. D. Intracranial saccular aneurysms. *Biomechanics of Soft Tissue in Cardiovascular Systems*, Springer Wien, New York (2003)

[7] David, G. and Humphrey, J. D. Further evidence for the dynamic stability of intracranial saccular aneurysms. *Journal of Biomechanics* **36**(7), 1043–1150 (2003)

[8] Humphrey, J. D. and Canham, P. B. Structure, mechanical properties, and mechanics of intracranial saccular aneurysms. *Journal of Elasticity* **61**(1-3), 49–81 (2000)

[9] Kroon, M. and Holzapfel, G. A. Estimation of the distributions of anisotropic, elastic properties and wall stresses of saccular cerebral aneurysms by inverse analysis. *Proceedings of the Royal Society A*: *Mathematical*, *Physical and Engineering Sciences* **464**(6), 807–825 (2008)

[10] Holzapfel, G. A., Gasser, T. C., and Stadler, M. A structural model for the viscoelastic behavior of arterial walls: continuum formulations and finite element analysis. *European Journal of Mechanics A/Solids* **21**(3), 441–463 (2002)

[11] Taber, L. A. *Nonlinear Theory of Elasticity*: A*pplications in Biomechanics*, World Scientific Publishing Company, New Jersy (2004)

[12] Holzapfel, G. A., Gasser, T. C., and Ogden, R. W. A new constitutive framework for arterial wall mechanics and a comparative study of material models. *Journal of Elasticity* **61**(1-3), 1–48 (2000)

[13] Holzapfel, G. A., Sommer, G., and Regitnig, P. Anisotropic mechanical properties of tissue components in human atherosclerotic plaques. *Journal of Biomechanical Engineering* **126**(5), 657–665 (2004)

[14] Driessen, N. J. B., Wilson, W., Bouten, C. V. C., and Baaijens, F. P. T. A computational model for collagen fiber remodeling in the arterial wall. *Journal of Theoretical Biology* **226**(1), 53–64 (2004)

[15] Gasser, T. C., Ogden, R. W., and Holzapfel, G. A. Hyperelastic modeling of arterial layers with distributed collagen fiber orientations. *Journal of the Royal Society Interface* **3**(1), 15–35 (2006)

[16] Vito, R. P. and Dixon, S. A. Blood vessel constitutive models — 1995–2002. *Annual Review of Biomedical Engineering* **5**(4), 413–439 (2003)

[17] Fung, Y. C. *Biomechanics*: *Motion*, *Flow*, *Stress and Growth*, Springer-Verlag, New York (1990)

[18] Baek, S., Gleason, R. L., Rajagopal, K. R., and Humphrey, J. D. Theory of small on large: potential utility in computations of fluid-solid interactions in arteries. *Computer Methods in Applied Mechanics and Engineering* **196**(15), 3070–3078 (2007)

[19] Masson, I., Boutouyrie, P., Laurent, S., Humphrey, J. D., and Zidi, M. Characterization of arterial wall mechanical behavior and stresses from human clinical data. *Journal of Biomechanics* **41**(12), 2618–2627 (2008)

[20] Vena, P., Gastadi, D., Socci, L., and Pennati, G. An anisotropic model for tissue growth and remodeling during early development of cerebral aneurysms. *Computational Materials Science* **43**(3), 565–577 (2008)

[21] Baek, S., Rajagopal, K. R., and Humphrey, J. D. A theoretical model of enlarging intracranial fusiform aneurysm. *Journal of Biomechanical Engineering* **128**(1), 142–149 (2006)

[22] Haughton, D. M. and Ogden, R. W. On the incremental equations in non-linear elasticity-II: bifurcation of pressurized spherical shells. *Journal of the Mechanics and Physics of Solids* **26**(2), 111–138 (1978)

[23] Kroon, M. and Holzapfel, G. A. A theoretical model for fibroblast-controlled growth of saccular cerebral aneurysms. *Journal of Theoretical Biology* **257**(1), 73–83 (2009)

[24] Holzapfel, G. A., and Gasser, T. C. Computational stress-deformation analysis of arterial walls including high-pressure response. *International Journal of Cardiology* **116**(1), 78–85 (2007)